Research Article

Rapid Microwave Method to Enhance the Characteristics of Fe_3O_4 and Fe_3O_4/SiO_2 Nanoparticles

Lety Trisnaliani
Doctoral Program of Engineering Science, Faculty of Engineering, Universitas Sriwijaya, Inderalaya, Indonesia

Sri Haryati and Muhammad Djoni Bustan*
Department of Chemical Engineering, Faculty of Engineering, Universitas Sriwijaya, Inderalaya, Indonesia

* Corresponding author. E-mail: muhammaddjonibustan@ft.unsri.ac.id DOI: 10.14416/j.asep.2024.06.010
Received: 31 January 2024; Revised: 23 March 2024; Accepted: 28 May 2024; Published online: 26 June 2024

Abstract
The application of nanoparticles can increase the number of products and protect against the deadly effects of industrial processes. Generally, nanoparticle technology offers numerous benefits, including reduced energy consumption and waste generation. Therefore, this study aimed to prepare Fe_3O_4 and Fe_3O_4/SiO_2 nanoparticles using rapid microwave method. The instruments used for analysis included x-ray diffraction (XRD), Fourier transform infrared spectroscopy (FT-IR), vibrating sample magnetometer (VSM), scanning electron microscopy-dispersive x-ray (SEM-EDX), and ultraviolet-visible diffuse reflectance spectroscopy (UV-DRS). The combustion process was carried out using a microwave to produce sufficient energy for forming Fe_3O_4 nanoparticles. The homogeneous heating distribution process in the raw material effectively formed different initial phases and nanoparticle morphologies within a few minutes. The results showed that the application of rapid and efficient microwave provided good monodispersity, uniform core-shell structure, and high magnetization. The calculated optical bandgap values for Fe_3O_4 and Fe_3O_4/SiO_2 ranged from 1.77–2.33 eV. According to magnetic analysis, Fe_3O_4 nanoparticles showed superparamagnetic behavior at room temperature with a value of 32–40 emu/g, while Fe_3O_4/SiO_2 powder had 9–23 emu/g. The analysis of SEM-EDX showed that SiO_2 had the potential to prevent particle aggregation and stabilize the nanoparticles prepared. Moreover, further study is recommended to modify the product with other materials, such as TiO_2, for photocatalysts.

Keywords: Magnet, Microwave, Nanocatalyst, Optic, SiO_2, Structure

1 Introduction

According to a global study, the discovery of lodestone is widely recognized as the mineral magnetite (Fe_3O_4) [1]. The term 'magnet' originated from the region where this magnetic stone was found, namely Magnesia (Anatolia) [2], [3]. In chemistry and mineralogy, magnetic stone is magnetite, an iron ore with strong remanent magnetization [4]. Additionally, magnetite is typical of semiconductors, showing potential as a catalyst capable of minimizing micro-organisms [5]. This significant potential and the ability to absorb metal materials is an advantage of Fe_3O_4 nanoparticles [6]. Other advantages of iron oxide include biocompatibility, friendly environment, suitability for drug delivery, low toxicity, electromagnetic ability, and biomedical applications [7], [8]. Several new technological developments have investigated the characteristics and properties, specifically focusing on the shape and size of Fe_3O_4 crystals [9]–[15]. Some preparations have produced Fe_3O_4 nanostructures, including coprecipitation, hydrothermal, micro-emulsion, sol-gel, ultrasonic, and biological synthesis [16]–[21]. However, all these preparations have some limitations due to relatively low yields, long synthesis times, and requirements for organic solvents [22]. Several alternatives have

been developed to address this limitation, including sonochemical method for preparing the core-shell structure of Fe_3O_4 nanoparticles, using solvothermal to synthesize the superparamagnetic iron oxide nanorods [23] or using solvothermal to synthesize the superparamagnetic iron oxide nanorods [24]. Other studies have successfully synthesized Fe_3O_4 using the coprecipitation method with different reaction temperatures, high crystallinity, and spherical shape [25]. Another report explained that a liquid thermal decomposition method was prepared to produce colloidal Fe_3O_4 nanoparticles of regulated size [26]. The inverse microemulsion method has proven effective in thickening the silica layer to protect the nanomagnetics from aggregation properties. Nanoparticle alloys have been prepared through Stöber precipitation and modification methods, facilitating the synthesis of magnetic iron oxide (Fe_3O_4) and Fe_3O_4/SiO_2 core shells applied in nonlinear optics [27]. Despite these advantages, conventional methods often entailed time-intensive procedures to prepare Fe_3O_4. A recent study explained that Fe_3O_4 nanoparticles were prepared using hydrothermal methods at 160–200 °C for six hours [28]. However, these methods are expensive and complex, including handling significant volumes of organic matter, surfactant solvents, and environmental pollution rather than producing highly purified Fe_3O_4. This phenomenon shows the need for a new method that is faster, more efficient, and environmentally friendly, preserving the structure of Fe_3O_4 nanoparticles. Therefore, this study used a microwave to synthesize Fe_3O_4 and Fe_3O_4/SiO_2 nanoparticles. Synthesis of high-performance magnetite nanoparticles can be achieved quickly and easily due to modern microwave chemistry, which has several advantages compared to conventional methods [29]. This microwave and precursor material interaction promotes a fast and uniform heating process due to the penetrating quality of irradiation [30], [31]. During the process, energy transfers from hot conditions into rapid kinetic movements, leading to homogeneous volume heating to produce nanoparticles due to irradiation and molecular reactions [32]. For example, iron oxide nanoparticles have been rapidly produced using microwave, polyethylene glycol (PEG), aqueous ferric chloride salt, and ammonia. The main determinants of the dimensional properties of nanoparticles are heating time, microwave power, and PEG. The characteristics of nanoparticles have also been recognized using X-ray Diffraction (XRD), Transmission Electron Microscopy (TEM), Fourier Transform Infrared spectroscopy (FT-IR), Vibrating Sample Magnetometer (VSM), X-ray Photoelectron Spectroscopy (XPS), and Thermo Gravimetric (TG) [33]. In another method, hematite was produced using alkaline media and 0.1 M $FeCl_3$ solution as a precursor, followed by heating at 800 W for 20 min, with temperatures fluctuating between 150, 200, and 250 °C. Horikoshi *et al.*, stated that the use of microwaves during synthesis could produce nanoparticles with homogeneous shapes and sizes more quickly, cheaply, and effectively compared to the conventional high-temperature annealing method [34]. However, Fe_3O_4 nanoparticles have limitations, including susceptibility to agglomeration, large surface area, chemical reactivity, and high surface energy, leading to potential loss of magnetic properties [35], [36]. Modifications such as coating have been proven effective by combining metal and non-metal materials, preparing nanostructures, and using coating (template) strategies to overcome the limitations [37], [38]. The coating method is used to conjugate organic or inorganic materials onto the iron oxide surface [39]. This modification avoids oxidation and agglomeration events, thereby improving the physicochemical properties of Fe_3O_4 nanoparticles and increasing functionality as an ideal catalysis material [40]. Several studies have added other materials to prepare Fe_3O_4 composites, such as coating Ag nanoparticles on magnetite [41], magnetite polydimethylsiloxane composite [42], carbon-coated Fe_3O_4 [43], [44], and SiO_2 [45]–[48]. Among these materials, previous reports show that SiO_2 had significant potential due to high thermal resistance, physical and chemical stability, the ability to maintain surface hydroxyl groups, biocompatibility, non-toxicity, and inert nature [49]. In this study, SiO_2 was used to coat Fe_3O_4 nanoparticles to adjust the pore structure and size [50]. The synthesis process also included the use of ferric chloride hexahydrate ($FeCl_3.6H_2O$), ferrous chloride tetrahydrate ($FeCl_2.4H_2O$), and pH modifiers with sodium hydroxide (NaOH) to produce magnetic (Fe_3O_4) nanoparticles. Structure and size of the crystals were also determined, along with functional groups and the optical band gap of the synthesized compounds. This characterization process was carried out using XRD, FT-IR, VSM, Scanning Electron Microscopy-

Dispersive X-ray (SEM-EDX), and Ultraviolet-Visible Diffuse Reflectance Spectroscopy (UV-DRS).

2 Experimental

2.1 *Preparation of Fe_3O_4 and Fe_3O_4/SiO_2 nanoparticles*

Magnetite samples were produced quickly using an effective microwave method. All materials used were purchased from Merck Millipore Indonesia and applied without preprocessing. These included ferric chloride hexahydrate ($FeCl_3.6H_2O$), ferrous chloride tetrahydrate ($FeCl_2.4H_2O$), sodium hydroxide (NaOH), tetraethyl orthosilicate (TEOS), ethanol, ammonia solution (26% w/v). Iron oxide nanoparticles were prepared using a rapid microwave in an alkaline solution. Initially, 15 mL of deionized water was heated to a temperature of 75 °C, mixed with $FeCl_3.6H_2O$ (1 g) and $FeCl_2.4H_2O$ (2 g). Subsequently, the mixture was added with 3 M NaOH (100 mL) and stirred for 1 h in a silica crucible. After the stirring treatment, the suspension was placed with a silica crucible into a microwave oven (400 W) and irradiated for 10 min. The procedure of Fe_3O_4 nanoparticle synthesis used a 400 W microwave at 60, 100, and 140 °C temperatures. The product was obtained as nanoparticles with a small crystal size, and the solution was brought to a boil, where dehydration and decomposition occurred, leading to solidification. The solids obtained were labeled as A1 (Fe_3O_4, T = 60 °C), A2 (Fe_3O_4, T = 100 °C), and A3 (Fe_3O_4, T = 140 °C), which were subjected to further treatment using a permanent magnet. The dark precipitates were washed several times with deionized water to remove residual ions and dried at 60 °C for two hours. For the experiment of Fe_3O_4/SiO_2, TEOS, ammonia solution (26% w/v), ethanol, and deionized water were prepared and stirred in the silica crucible, following the same procedure for Fe_3O_4. In this process, 0.5 g of dried Fe_3O_4 was dispersed in ethanol, deionized water, and a 26 % ammonia solution. The suspension was ultrasonicated for 30 min, 10 mL of TEOS to magnetite solution was added, and stirred for 15 min. An external magnet was used to facilitate the separation of Fe_3O_4/SiO_2 from the suspension, which was washed three times and dried in an oven at 60 °C for two hours. The products obtained were denoted as B1 (Fe_3O_4/SiO_2, T = 60 °C), B2 (Fe_3O_4/SiO_2, T = 100 °C), and B3 (Fe_3O_4/SiO_2, T = 140 °C).

2.2 *Characterization of Fe_3O_4 and Fe_3O_4/SiO_2 nanoparticles*

All samples prepared were analyzed using a Rigaku Miniflex-600 XRD X-ray diffractometer with Cu Kα radiation at λ = 1.5406 Å. Structural refinements using the Rietveld method were carried out using Match software. Subsequently, the Nicolet Avatar 360 FT-IR spectrometer was used to analyze the surface functional groups. The energy-dispersive X-ray analysis of Fe_3O_4 and Fe_3O_4/SiO_2 samples was performed with Phenom Desktop ProXL scanning electron microscopy to identify the morphology. The diffuse reflectance UV- DRS spectrum was recorded using Pharmaspec 1700 to estimate band gap energy. The magnetization was analyzed by determining magnetic properties using Oxford 1.2 H VSM.

3 Result and Discussions

3.1 *XRD analysis*

The crystal structure of Fe_3O_4 and Fe_3O_4/SiO_2 nanoparticle products was identified using an X-ray diffractometer to determine the average size of single-crystal nanoparticles. XRD patterns can be calculated using the Debye-Scherrer equation [51].

$$D = 0.98\ \lambda/\beta\ cos\ \theta \quad (1)$$

The crystal size of nanoparticles is denoted by D, Scherrer constant (0.98), the X-ray wavelength (λ = 1.54), the Bragg diffraction angle (θ), and β is the symbol for half of the maximum full width (FWHM). Figure 1 shows XRD with various diffraction peaks of Fe_3O_4 and Fe_3O_4/SiO_2. The characteristic spectrum of standard Fe_3O_4 are 31.69 (220), 35.54 (311), 43.38 (400), 55.01 (422), 57.14 (511), and 62.78 (440). The peak existed at 2θ = 21.94 (200), which might be attributed to amorphous SiO_2. The XRD peaks indicated that the crystal structure of Fe_3O_4 nanoparticles did not change during the modification process. The addition of SiO_2 did not affect the physical properties of Fe_3O_4 nanoparticles. A previous study has established that magnetic phase Fe_3O_4 can be superparamagnetic or ferromagnetic [52]. All diffraction peaks can be indexed to the pure cubic phase (JCPDS 96–900-2319), showing the crystalline nature of the synthesized

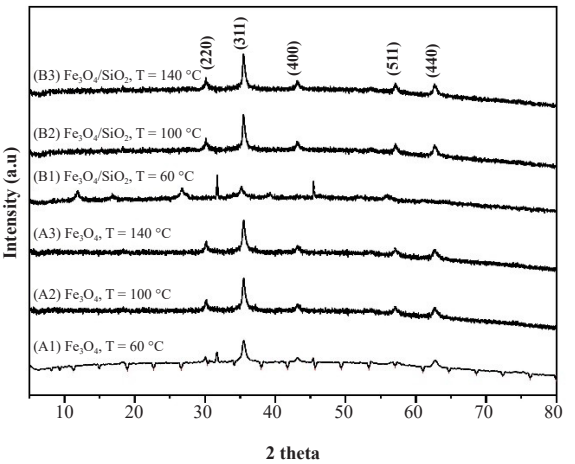

Figure 1: XRD pattern : (A1) Fe_3O_4, T = 60 °C; (A2) Fe_3O_4, T = 100 °C; (A3) Fe_3O_4, T = 140 °C; (B1) Fe_3O_4/SiO_2, T = 60 °C; (B2) Fe_3O_4/SiO_2, T = 100 °C; (B3) Fe_3O_4/SiO_2, T = 140 °C.

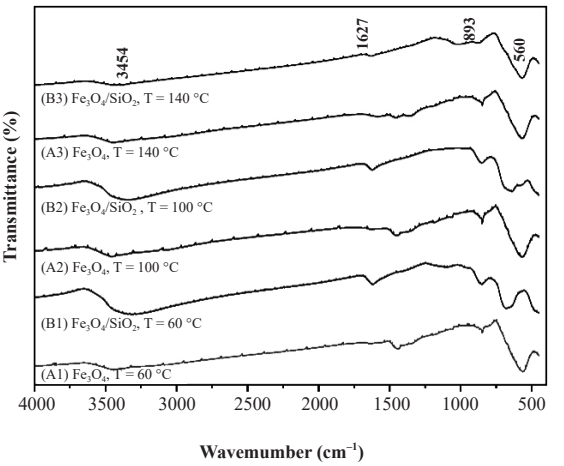

Figure 2: FTIR spectra : (A1) Fe_3O_4, T = 60 °C ; (B1) Fe_3O_4/SiO_2, T = 60 °C; (A2) Fe_3O_4, T = 100 °C; (B2) Fe_3O_4/SiO_2 , T = 100 °C; (A3) Fe_3O_4, T = 140 °C; (B3) Fe_3O_4/SiO_2, T = 140 °C.

material. Although the amorphous SiO_2 layer on top has no impact on the magnetism structure of Fe_3O_4 [53], the presence of silica groups will result in a larger Fe_3O_4 crystal size. This study produced magnetic nanoparticles in a microwave oven operating at 400 W with 60, 100, and 140 °C temperatures, forming Fe_3O_4 nanoparticles within 10 min.

3.2 *FT-IR spectra*

Figure 2 shows the FT-IR spectra for Fe_3O_4 and Fe_3O_4/SiO_2, where the main band for Fe_3O_4 was identified around 552–571 cm^{-1}, as indicated by the Fe-O stretching vibration [54]. Fe_3O_4/SiO_2 group was shown at 1620–1627 cm^{-1}, associated with the stretching vibrations of the Si-O-Si bonds due to oxygen transport [55]. The absorption band at 3447–3454 cm^{-1} was associated with OH groups from the hydroxyl group bonded to Si (Si-OH). Moreover, both Fe_3O_4 and Fe_3O_4/SiO_2 have been observed as the cubic type [56].

3.3 *VSM-curves*

The magnetic properties of Fe_3O_4 shown in Figure 3 are combined with SiO_2 to obtain the saturation magnetization value. SiO_2 encapsulates Fe_3O_4, reducing the highest saturation magnetization observed at 9–23 emu/g compared to Fe_3O_4 at 32, 38, and 40 emu/g. This significant reduction is attributed to several factors, including impurities, crystallinity, and particle size [57]. The characterization results show that artificial Fe_3O_4/SiO_2 has lower magnetic properties than Fe_3O_4 nanoparticles.

3.4 *SEM-EDX analysis*

SEM-EDX analysis was used to analyze the morphological structure of Fe_3O_4 and Fe_3O_4/SiO_2 nanocomposites. Figure 4 (A1, A2, and A3) shows the SEM-EDX images, indicating the micromorphology of Fe_3O_4 at 5000x magnification. Fe_3O_4 nanoparticles show 8 and 10 µm lengths and concentrations of elemental O (37.33%) and Fe (37.00%). Due to the tiny size and magnetic power, Fe_3O_4 nanoparticles have an unsymmetrical crystal shape, with surface morphology showing the aggregation of numerous nanoscale particles [58]. Furthermore, Figure 4 (B1, B2, and B3) shows that Fe_3O_4 magnetic nanoparticles have SiO_2 layers [59]. The nanocomposite components show a higher concentration of Fe (53.64%) and O (36.71%). Specifically, a significant amount of Fe is detected on the outermost layer of Fe_3O_4/SiO_2, suggesting the precipitation of Sodium (Na).

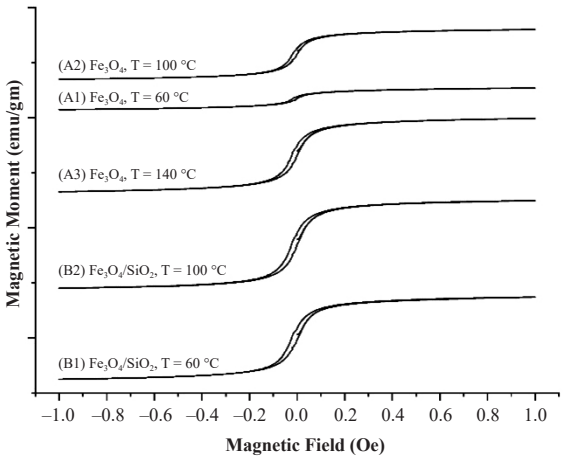

Figure 3: The VSM curve: (A1) Fe_3O_4 (60 °C); (A2) Fe_3O_4 (100 °C); (A3) Fe_3O_4 (140 °C); (B1) Fe_3O_4/SiO_2 (60 °C); (B2) Fe_3O_4/SiO_2 (100 °C).

Table 1: Elemental composition of Fe_3O_4 and Fe_3O_4/SiO_2

No.	Element Symbol	Element Name	Weight Conc. Fe_3O_4	Weight Conc. Fe_3O_4/SiO_2
1	O	Oxygen	37.33	53.64
2	Fe	Iron	37.00	36.71
3	Na	Sodium	18.83	6.58
4	C	Carbon	5.77	1.40
5	Cl	Chlorine	0.63	1.18
6	Si	Silicon	0.44	0.49

This phenomenon is facilitated by using sodium hydroxide (NaOH) to accelerate the deposition process. Additionally, chlorine is assumed to be present in Fe_3O_4 and SiO_2 to form $FeCl_3$ and $FeCl_2$, respectively. Table 1 lists the constituent elements of Fe_3O_4 and Fe_3O_4/SiO_2.

3.5 *Optical properties by DRS studies*

The Tauc Plot method calculates the energy band gap (optical properties) [60]. For semiconductor materials, the formula used is expressed as follows.

$$(\alpha.h\upsilon)^{1/\gamma} = B(h\upsilon - Eg) \quad (2)$$

In this study, the energy band gap sequences in the synthesis of Fe_3O_4 are 2.33 (T = 60 °C), 2.15 (T = 100 °C), and 2.11 (T = 140 °C), while Fe_3O_4/SiO_2

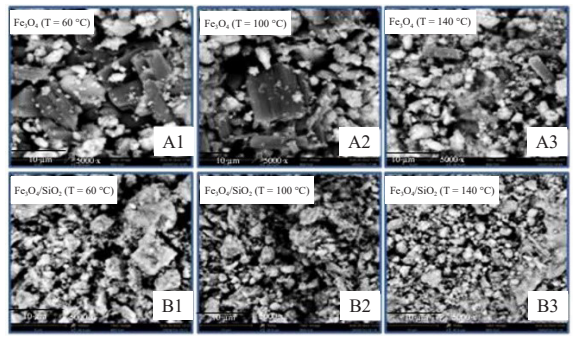

Figure 4: SEM-EDX of Fe_3O_4 (A1 (T = 60 °C), A2 (T = 100 °C) and A3 (T = 140 °C)) and Fe_3O_4/SiO_2 (B1 (T = 60 °C), B2 (T = 100 °C) and B3 (T = 140 °C)).

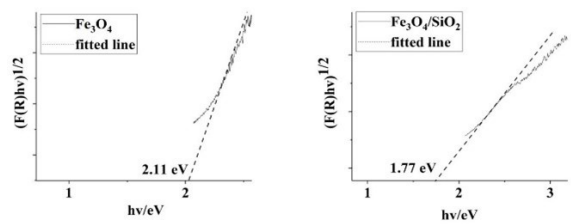

Figure 5: Tauc plot method of (A3) Fe_3O_4, T = 140 °C (2.11 eV) and (B3) Fe_3O_4/SiO_2, T = 140 °C (1.77 eV).

is 2.04 (T = 60 °C), 2.03 (T = 100 °C), and 1.77 eV (T = 140 °C), respectively. As shown in Figure 5, Fe_3O_4 and Fe_3O_4/SiO_2 nanoparticles in microwave synthesis at 140 °C have estimated band gaps of 2.11 and 1.77 eV, respectively. The sample energy gap decreases due to increased TEOS content, while particle size is inverse to the selection band gap energy. The conduction band density shows significant variation due to the inverse ratio between the band gap energy and the particle size. The transfer of electrons from the valence band to the conduction band requires a band gap energy value. Moreover, when the band gap increases, the energy value to activate electrons also rises, facilitating the absorption of low wavelengths [61], [62].

4 Conclusions

In conclusion, this study successfully synthesized Fe_3O_4 and Fe_3O_4/SiO_2 nanoparticles using rapid microwave method. The advantages of microwave irradiation sources for chemical transformations included accelerated reaction rates, minimum energy consumption, and the absence of prolonged reflux

compared to the conventional method. This synthesis method was found suitable for the study conditions, which required a fast, safe, and environmentally friendly modern technology to heat the substrate for 10 min at reaction temperature conditions of 60–140 °C. The nature of Fe_3O_4, easily oxidized and aggregated during the preparation and application process, made SiO_2 the most potential candidate for coating Fe_3O_4 nanoparticles. SiO_2 compounds are chemically and thermally stable materials capable of protecting the surface of iron oxide nanoparticles. Furthermore, SiO_2 is non-toxic, soluble in water and well-compatible. Based on the results, the XRD pattern showed the formation of Fe_3O_4 and Fe_3O_4/SiO_2 structures, while the presence of functional groups was confirmed by FT-IR analysis. Electron microscopy showed the impact of surface modification on the morphology of the shape and size of nanoparticles, which increased from approximately 2.19 nm to 3.71 nm after SiO_2 coating. The saturation magnetization of Fe_3O_4/SiO_2 (9–23 emu/g) was lower than Fe_3O_4 (32–40 emu/g), showing successful templating of SiO_2 with Fe_3O_4. Analysis of the VSM curve confirmed that both Fe_3O_4 and Fe_3O_4/SiO_2 nanoparticles showed superparamagnetic behavior. The band gap also showed that Fe_3O_4 and Fe_3O_4/SiO_2 at a temperature of 140 °C have the smallest band gap energy, 2.11 and 1.77 eV, respectively. The addition of SiO_2 caused the band gap energy in the sample to become smaller. Generally, a small band gap value requires less energy for excited electrons to absorb light and wavelengths during photocatalysis, enhancing the potential of Fe_3O_4/SiO_2 nanoparticles as effective nanocatalysts. The result revealed that the Fe_3O_4/SiO_2 had better thermal stability and dispersion than the magnetite (Fe_3O_4) nanoparticles. The Fe_3O_4/SiO_2 nanoparticles benefit from a simple preparation method, cost-effectiveness, a short reaction time, excellent yield, friendly environment, high magnetization, and easy work-up, which are the main advantages of the present method. These results also demonstrated the suitability of Fe_3O_4/SiO_2 nanoparticles as promising materials for further investigations due to the safe and rapid synthesis process.

Acknowledgments

We extend our sincere thanks to BPPDN 2019 Doctoral Scholarships from the Higher Education General Director (Dirjen Dikti) of the Ministry of Education, Culture, Research, and Technology (Kemendikbud-Ristek) of the Republic of Indonesia.

Author Contributions

L.T.: investigation, methodology, writing an original draft, editing; S.H.: research design, data analysis; M.D.B.: conceptualization, data curation, reviewing. All authors have read and agreed to the published version of the manuscript.

Conflicts of interest

The authors declare that they have no conflicts of interest or personal relationships that could have appeared to influence the work reported in this paper.

References

[1] P. Wasilewski and G. Kletetschka, "Iron ore to lodestone: With lightning assist," *Journal of Applied Geophysics*, vol. 219, 2023, Art. no. 105225.

[2] A. A. Mills, "The Lodestone: History, physics, and formation," *Annals of Science*, vol. 61, no. 3, 2004, Art. no. 273.

[3] D. W. E. Systems and E. Nsw, "The lodestone, from plato to kircher the lodestone, from plato to kircher," *Preview*, vol. 2471, no. 2014, 2019.

[4] A. K. Vishwakarma, B. S. Yadav, A. K. Singh, S. Kumar, and N. Kumar, "Magnetically recyclable ZnO coated Fe_3O_4 nanocomposite for MO dye degradation under UV-light irradiation," *Solid State Sciences*, vol. 145, 2023, Art. no. 107312.

[5] A. Halfadji, M. Naous, K. nadia Kharroubi, F. el zahraà Belmehdi, and S. Rajendrachari, "An ultrasonic-assisted synthesis, characterization, and application of Nano-Fe_3O_4/TiO_2 as nano-catalyst for the removal of organic dye by Like-Photo-Fenton reactions," *Inorganic Chemistry Communications*, vol. 158, 2023, Art. no. 111686.

[6] X. Tian, X. Xu, G. Bo, X. Su, J. Yan, and Y. Yan, "A 3D flower-like Fe_3O_4@PPy composite with core-shell heterostructure as a lightweight and efficient microwave absorbent," *Journal of Alloys and Compounds*, vol. 923, 2022, Art. no. 166416.

[7] F. Bojabady, E. Kamali-Heidari, and S. Sahebian,

"Hydrothermal synthesis of highly aligned Fe_3O_4 nanosplates on nickel foam," *Materials Chemistry and Physics*, vol. 305, 2023, Art. no. 127828.

[8] N. Acharya, "Magnetically driven MWCNT-Fe_3O_4-water hybrid nanofluidic transport through a micro-wavy channel: A novel MEMS design for drug delivery application," *Materials Today Communications*, vol. 38, 2024, Art. no. 107844.

[9] L. Zhang, G. Song, Y. Song, J. Li, Z. Li, X. Yang, Z. Li, X. Li, and Z. Jia, "Ultralight 3D cross-linked reinforced graphene@Fe_3O_4 composite aerogels for electromagnetic wave absorption," *Materials Research Bulletin*, vol. 173, May 2024, Art. no. 112696.

[10] T. Hai, K. Sharma, R. K. Marjan, B. Farhang, M. H. Mahmoud, H. Fouad, and W. El-Shafai, "Numerical analysis of the magnetic field impact on hydrothermal characteristics of a microchannel heatsink with Fe_3O_4 ferrofluid and various pin-fin shapes," *Journal of Magnetism and Magnetic Materials*, vol. 585, 2023, Art. no. 171102.

[11] D. Rajkumar, A. Subramanyam Reddy, P. V Satya Narayana, K. Jagadeshkumar, and A. J. Chamkha, "Pulsating magnetohydrodynamic flow of Fe_3O_4-blood based micropolar nanofluid between two vertical porous walls with Cattaneo–Christov heat flux and entropy generation," *Journal of Magnetism and Magnetic Materials*, vol. 571, 2023, Art. no. 170564.

[12] K. Wang, X. Xu, Y. Li, M. Rong, L. Wang, L. Lu, J. Wang, F. Zhao, B. Sun, and Y. Jiang, "Preparation Fe_3O_4@chitosan-graphene quantum dots nanocomposites for fluorescence and magnetic resonance imaging," *Chemical Physics Letters*, vol. 783, 2021, Art. no. 139060.

[13] V. Vatanpour, S. Paziresh, A. H. Behroozi, H. Karimi, M. S. Esmaeili, S. Parvaz, S. I. Ghazanlou, and A. Maleki, "Fe_3O_4@Gum Arabic modified polyvinyl chloride membranes to improve antifouling performance and separation efficiency of organic pollutants," *Chemosphere*, vol. 328, 2023, Art. no. 138586.

[14] Y. Zhang, B. Su, Y. Tian, Z. Yu, X. Wu, J. Ding, C. Wu, D. Wei, H. Yin, J. Sun, and H. Fan, "Magnetic manipulation of Fe_3O_4@$BaTiO_3$ nanochains to regulate extracellular topographical and electrical cues," *Acta Biomaterialia*, vol. 168, 2023, Art. no. 470.

[15] A. G. Roca, L. Gutiérrez, H. Gavilán, M. E. Fortes Brollo, S. Veintemillas-Verdaguer, and M. del P. Morales, "Design strategies for shape-controlled magnetic iron oxide nanoparticles," *Advanced Drug Delivery Reviews*, vol. 138, 2019, Art. no. 68.

[16] I. Nkurikiyimfura, Y. Wang, B. Safari, and E. Nshingabigwi, "Temperature-dependent magnetic properties of magnetite nanoparticles synthesized via coprecipitation method," *Journal of Alloys and Compounds*, vol. 846, 2020, Art. no. 156344.

[17] J. M. M. Silva, P. E. Feuser, R. Cercená, M. Peterson, and A. G. Dal-Bó, "Obtention of magnetite nanoparticles via the hydrothermal method and effect of synthesis parameters," *Journal of Magnetism and Magnetic Materials*, vol. 580, 2023, Art. no. 170925.

[18] X. Qiao, A. Liu, Z. Li, J. Fan, P. Fan, and M. Fan, "Preparation and properties of dodecylamine microemulsion for the flotation of quartz and magnetite," *Minerals Engineering*, vol. 164, 2021, Art. no. 106821.

[19] M. B. Polla, J. L. Nicolini, J. Venturini, A. da Cas Viegas, M. A. Zen Vasconcellos, O. R. K. Montedo, and S. Arcaro, "Low-temperature sol–gel synthesis of magnetite superparamagnetic nanoparticles: Influence of heat treatment and citrate–nitrate equivalence ratio," *Ceramics International*, vol. 49, no. 5, 2023, Art. no. 7322.

[20] M. Haghmohammadi, N. Sajjadi, A. A. Beni, S. M. Hakimzadeh, A. Nezarat, and S. D. Asl, "Synthesis of activated carbon/magnetite nanocatalyst for sono-Fenton-like degradation process of 4-chlorophenol in an ultrasonic reactor and optimization using response surface method," *Journal of Water Process Engineering*, vol. 55, 2023, Art. no. 104216.

[21] A. Kilic, M. Emin Karatas, L. Beyazsakal, and V. Okumus, "Preparation and spectral studies of boronate ester modified magnetite iron nanoparticles (Fe_3O_4@APTES-B) as a new type of biological agents," *Journal of Molecular Liquids*, vol. 361, 2022, Art. no. 119602.

[22] G. Zanchettin, G. da S. Falk, S. Y. G. González, and D. Hotza, "High performance magnetically recoverable Fe_3O_4 nanocatalysts: Fast microwave synthesis and photo-fenton catalysis under

visible-light," *Chemical Engineering and Processing - Process Intensification*, vol. 166, 2021, Art. no. 108438.

[23] A. R. P. Hidayat, L. L. Zulfa, N. Faaizatunnisa, D. Prasetyoko, D. Hartanto, N. Widiastuti, A. S. Purnomo, M. Jannah, E. N. Kusumawati, H. Bahruji, and R. Ediati, "Properties and performance of Ni(II) doped magnetic Fe_3O_4@ mesoporous SiO_2/UiO-66 synthesized by an ultrasound assisted method for potential adsorbent of methyl orange: Kinetic, isotherm and thermodynamic studies," *Nano-Structures & Nano-Objects*, vol. 37, 2024, Art. no. 101077.

[24] R. Yang, B. Liang, D. Han, Z. Guo, C. Yang, J. Yang, Y. Qiu, Q. Li, S. Guo, J. Shi, X. Zhou, T. Qiang, and T. Guo, "Synthesis and antibacterial activity of magnetic Fe_3O_4-loaded silver nanocomposites," *Journal of Alloys and Compounds*, vol. 973, 2024, Art. no. 172849.

[25] G. Antarnusa, A. Esmawan, P. Dwi Jayanti, S. Rizki Fitriani, A. Suherman, E. Kinarya Palupi, R. Umam, and Ardimas, "Synthesis of Fe_3O_4 at different reaction temperatures and investigation of its magnetic properties on giant magnetoresistance (GMR) sensors for bio-detection applications," *Journal of Magnetism and Magnetic Materials*, vol. 563, 2022, Art. no. 169903.

[26] M. Sajid, S. Shuja, H. Rong, and J. Zhang, "Size-controlled synthesis of Fe_3O_4 and Fe_3O_4@ SiO_2 nanoparticles and their superparamagnetic properties tailoring," *Progress in Natural Science: Materials International*, vol. 33, no. 1, 2023, Art. no. 116.

[27] A. Khalid, R. M. Ahmed, M. Taha, and T. S. Soliman, "Fe_3O_4 nanoparticles and Fe_3O_4 @SiO_2 core-shell: Synthesize, structural, morphological, linear, and nonlinear optical properties," *Journal of Alloys and Compounds*, vol. 947, 2023, Art. no. 169639.

[28] M. Periyasamy, S. Sain, U. Sengupta, M. Mandal, S. Mukhopadhyay, and A. Kar, "Bandgap tuning of photo Fenton-like Fe_3O_4/C catalyst through oxygen vacancies for advanced visible light photocatalysis," *Materials Advances*, vol. 2, no. 14, 2021, Art. no. 4843.

[29] S. Sharma, Tirath, S. Pandey, S. Azizov, and D. Kumar, "Chapter 8 - Microwave-assisted organic synthesis using nanoparticles," in *Advances in Green and Sustainable Chemistry*, S. Bhunia, B. Kumar, P. Singh, R. Oraon, and K.-H. B. T.-N. in G. O. S. Kim, Eds. Amsterdam, Netherlands: Elsevier, 2023. Art. no. 241.

[30] C. Luo, S. Liu, G. Yang, P. Jiang, X. Luo, Y. Chen, M. Xu, E. Lester, and T. Wu, "Microwave-accelerated hydrolysis for hydrogen production over a cobalt-loaded multi-walled carbon nanotube-magnetite composite catalyst," *Applied Energy*, vol. 333, 2023, Art. no. 120538.

[31] S. Harnsoongnoen, "Microwave sensors based on coplanar waveguide loaded with split ring resonators: A review," *Applied Science and Engineering Progress*, vol. 12, no. 4, pp. 224–234, 2019, doi: 10.14416/j.ijast.2018.11.006.

[32] A. Manikandan, J. J. Vijaya, J. A. Mary, L. J. Kennedy, and A. Dinesh, "Structural, optical and magnetic properties of Fe_3O_4 nanoparticles prepared by a facile microwave combustion method," *Journal of Industrial and Engineering Chemistry*, vol. 20, no. 4, 2014, Art. no. 2077.

[33] R. Jain, "Effect of gadolinium doping on the Structural, magnetic, Electrical, Optical, and elastic properties of magnetite nanoparticles," *Materials Science and Engineering: B*, vol. 296, 2023, Art. no. 116631.

[34] S. Horikoshi, H. Tanizawa, A. Sawai, and N. Serpone, "Low-temperature microwave-driven thermochemical generation of hydrogen from steam reforming of alcohols over magnetite," *International Journal of Hydrogen Energy*, vol. 47, no. 56, 2022, Art. no. 23520.

[35] S. S. Alterary and A. Alkhamees, "Synthesis, surface modification, and characterization of Fe_3O_4 @SiO_2 coreshell nanostructure," *Green Processing and Synthesis*, vol. 10, 2021, Art. no. 384.

[36] Yusmaniar, Erdawati, H. Sosiati, S. Budi, M. Alaydrus, and E. Handoko, "Microwave absorbing characteristics of Fe_3O_4 @ SiO_2 core – shell polyaniline-based composites," *Materials Research Express*, vol. 8, no. 4, 2021, Art. no. 46101.

[37] I. Gabelica, L. Ćurković, V. Mandić, I. Panžić, D. Ljubas, and K. Zadro, "Rapid microwave-assisted synthesis of Fe_3O_4/SiO_2/TiO_2 core-2-layer-shell nanocomposite for photocatalytic degradation of ciprofloxacin," *Catalysts*, vol. 11,

no. 10, 2021, Art. no. 1136.

[38] A. Hamisu and U. I. Gaya, "Bi-Template assisted sol-gel synthesis of photocatalytically-active mesoporous anatase," *Applied Science and Engineering Progress*, vol. 14, no. 3, pp. 313–327, 2021, doi: 10.14416/j.asep.2021.04.003.

[39] A. Karimova, S. Hajizada, H. Shirinova, S. Nuriyeva, and L. Gahramanli, "Surface modification strategies for chrysin-loaded iron oxide nanoparticles to boost their anti-tumor efficacy in human colon carcinoma cells," *Journal of Functional Biomaterials*, vol. 15, no. 2, 2024, Art. no. 43.

[40] F. Ahmad, M. M. Salem-bekhit, F. Khan, S. Alshehri, and A. Khan, "Unique properties of surface-functionalized nanoparticles for bio-application : Functionalization mechanisms and importance in application," *Nanomaterials*, vol. 12, no. 8, 2022, Art. no. 1333.

[41] D. Ghanbari, "Green synthesis of C@Fe_3O_4@Ag nanocomposites: Coating of silver nanoparticles on the carbon template / magnetite as a catalyst for conversion of toxic carbon monoxide to carbon dioxide," *Journal of Nanostructures*, vol. 11, no. 3, 2021, Art. no. 297.

[42] A. Chen, Q. Wang, M. Li, Z. Peng, J. Lai, J. Zhang, J. Xu, H. Huang, and C. Lei, "Combined approach of compression molding and magnetic attraction to micropatterning of magnetic polydimethylsiloxane composite surfaces with excellent anti-icing/deicing performance," *ACS Applied Materials & Interfaces*, vol. 13, no. 40, 2021, Art. no. 48153.

[43] D. Jiang, Y. Chen, K. Xie, S. Li, and Y. Wang, "Carbon-coated Fe_3O_4@cotton fiber biomass carbon for the oxygen reduction reaction in air cathode microbial fuel cells," *Journal of Alloys and Compounds*, vol. 982, 2024, Art. no. 173843.

[44] S. Ajmal, A. Kumar, G. Yasin, M. M. Alam, M. Selvaraj, M. Tabish, M. A. Mushtaq, R. K. Gupta, and W. Zhao, "A microwave-assisted decoration of carbon nanotubes with Fe_3O_4 nanoparticles for efficient electrocatalytic oxygen reduction reaction," *Journal of Alloys and Compounds*, vol. 943, 2023, Art. no. 169067.

[45] A. Diego-lopez, O. Cabezuelo, A. Vidal-moya, M. L. Marin, and F. Bosca, "Synthesis and mechanistic insights of SiO_2@WO_3@Fe_3O_4 as a novel supported photocatalyst for wastewater remediation under visible light," *Applied Materials Today*, vol. 33, no. July, 2023, Art. no. 101879.

[46] F. Sadegh, W. Wongniramaikul, and R. Apiratikul, "Environmental technology & innovation magnetically recyclable Fe_3O_4–CuS@SiO_2 catalyst for synergistic adsorption and photodegradation of methyl orange in wastewater under visible light," *Environmental Technology & Innovation*, vol. 33, 2024, Art. no. 103545.

[47] P. L. Hariani, S. Salni, M. Said, and R. Farahdiba, "Core-shell Fe_3O_4/SiO_2/TiO_2 magnetic modified ag for the photocatalytic degradation of congo red dye and antibacterial activity," *Bulletin of Chemical Reaction Engineering & Catalysis*, vol. 18, no. 2, 2023, Art. no. 315.

[48] S. Wardhani, H. A. Mardiansyah, and D. Purwonugroho, "Fe_3O_4-SiO_2-Alginate photocatalyst for textile dyes waste degradation," *Science and Technology Indonesia*, vol. 8, no. 1, pp. 108–115, 2023.

[49] S. Kamari and A. Shahbazi, "Biocompatible Fe_3O_4@SiO_2-NH_2 nanocomposite as a green nanofiller embedded in PES–nanofiltration membrane matrix for salts, heavy metal ion and dye removal: Long–term operation and reusability tests," *Chemosphere*, vol. 243, 2020, Art. no. 125282.

[50] H. Li, H. Jin, R. Li, J. Hua, Z. Zhang, and R. Li, " Magnetic Fe_3O_4@SiO_2 study on adsorption of methyl orange on nanoparticles," *Scientific Reports*, vol. 14, 2024, Art. no. 1217.

[51] U. Holzwarth and N. Gibson, "The scherrer equation versus the 'Debye-Scherrer equation,'" *Nature Nanotechnology*, vol. 6, no. 9, 2011, Art. no. 534.

[52] C. Xue, Q. Zhang, J. Li, X. Chou, W. Zhang, H. Ye, Z. Cui, and P. J. Dobson, "High photocatalytic activity of Fe_3O_4-SiO_2-TiO_2 functional particles with core-shell structure," *Journal of Nanomaterials*, vol. 2013, 2013, Art. no 762423.

[53] J. H. Cha, H.-H. Choi, Y.-G. Jung, S.-C. Choi, and G. S. An, "Novel synthesis of core–shell structured Fe_3O_4@SiO_2 nanoparticles via sodium silicate," *Ceramics International*, vol. 46, no. 10, 2020, Art. no. 14384.

[54] J. Mohapatra, A. Mitra, H. Tyagi, D. Bahadur, and M. Aslam, "Iron oxide nanorods as high-

performance magnetic resonance imaging contrast agents," *Nanoscale*, vol. 7, 2015, Art. no. 9174.

[55] R. Ellerbrock, M. Stein, and J. Schaller, "Comparing amorphous silica, short-range-ordered silicates and silicic acid species by FTIR," *Scientific Reports*, vol. 12, no. 1, 2022, Art. no. 11708.

[56] V. I. Simagina, O. V Komova, G. V Odegova, and O. V Netskina, "Study of copper – Iron mixed oxide with cubic spinel structure, synthesized by the combustion method," *Russian Journal of Applied Chemistry*, vol. 92, no. 1, 2019, Art. no. 20.

[57] Q. Li, C. W. Kartikowati, S. Horie, T. Ogi, T. Iwaki, and K. Okuyama, "Correlation between particle size/domain structure and magnetic properties of highly crystalline Fe_3O_4 nanoparticles," *Scientific Reports*, vol. 7, no. 1, 2017, Art. no. 1.

[58] D. Caruntu, G. Caruntu, Y. Chen, C. J. O'Connor, G. Goloverda, and V. L. Kolesnichenko, "Synthesis of variable-sized nanocrystals of Fe_3O_4 with high surface reactivity," *Chemistry of Materials*, vol. 16, no. 25, 2004, Art. no. 5527.

[59] Y. X. Zhang, X. Y. Yu, Z. Jin, Y. Jia, W. H. Xu, T. Luo, B. J. Zhu, J. H. Liu, and X. J. Huang, "Ultra high adsorption capacity of fried egg jellyfish-likeγAlOOH(Boehmite)@SiO_2/Fe_3O_4 porous magnetic microspheres for aqueous Pb(II) removal," *Journal of Materials Chemistry*, vol. 21, no. 41, 2011. Art. no. 16550.

[60] P. R. Jubu, F. K. Yam, V. M. Igba, and K. P. Beh, "Tauc-plot scale and extrapolation effect on bandgap estimation from UV–vis–NIR data – A case study of β-Ga_2O_3," *Journal of Solid State Chemistry*, vol. 290, 2020, Art. no. 121576.

[61] S. Anjum, R. Tufail, K. Rashid, R. Zia, and S. Riaz, "Effect of cobalt doping on crystallinity, stability, magnetic and optical properties of magnetic iron oxide nano-particles," *Journal of Magnetism and Magnetic Materials*, vol. 432, 2017, Art. no. 198.

[62] A. Nikmah, A. Taufiq, and A. Hidayat, "Synthesis and Characterization of Fe_3O_4/SiO_2 nanocomposites," *IOP Conference Series: Earth and Environmental Science*, vol. 276, no. 1, 2019, Art. no. 12046.